PROCEEDINGS OF SPIE

SPIEDigitalLibrary.org/conference-proceedings-of-spie

Evaluation of a cardiac flow phantom for absolute myocardial perfusion SPECT measurements

M. Kamphuis, Marcel J. W. Greuter, R. H. J. Slart, Cornelis Slump

M. E. Kamphuis, Marcel J. W. G. Greuter, R. H. J. A. Slart, Cornelis H. Slump, "Evaluation of a cardiac flow phantom for absolute myocardial perfusion SPECT measurements," Proc. SPIE 12036, Medical Imaging 2022: Biomedical Applications in Molecular, Structural, and Functional Imaging, 1203626 (4 April 2022); doi: 10.1117/12.2623667

SPIE.

Event: SPIE Medical Imaging, 2022, San Diego, California, United States

Evaluation of a cardiac flow phantom for absolute myocardial perfusion SPECT measurements

M.E. Kamphuis*[a,b], Marcel J.W.G. Greuter[b,c], Riemer J.H.A. Slart[d,e], Cornelis H. Slump[b]
[a]Multi-modality Medical Imaging Group, Faculty of Science and Technology, University of Twente, Enschede, the Netherlands; [b]Robotics and Mechatronics Group, Faculty of Electrical Engineering Mathematics and Computer Science, University of Twente, Enschede, the Netherlands; [c]Medical Imaging Centre, Department of Radiology, University Medical Center Groningen, University of Groningen, Groningen, the Netherlands; [d]Medical Imaging Centre, Department of Nuclear Medicine and Molecular Imaging, University Medical Center Groningen, University of Groningen, Groningen, the Netherlands; [e]Biomedical Photonic Imaging Group, Faculty of Science and Technology, Technical Medical Centre, University of Twente, Enschede, the Netherlands

ABSTRACT

Absolute myocardial perfusion imaging (MPI) can be beneficial in the diagnosis and prognosis of patients with coronary artery disease. However, validation and standardization of perfusion estimates across centers is needed to ensure safe and adequate integration into clinical routine. MPI phantoms can contribute to this clinical need as these models can provide ground truth evaluation of absolute MPI in a simplified, though controlled setup. This work presents verification of phantom design choices, including the justification for using sorbents in mimicking contrast kinetics (i.e., tracer uptake and retention). Moreover, we compare preliminary phantom results obtained with SPECT-MPI with a patient example. Finally, we applied a general two-tissue compartment model to describe the obtained phantom time activity curve data. These evaluation steps support shaping of a suitable verification and validation strategy for the multimodal myocardial perfusion phantom design and realization.

Keywords: phantom, model verification, quantitative imaging, myocardial perfusion, tracer kinetics, SPECT, ground truth

1. INTRODUCTION

1.1 Myocardial perfusion imaging

Myocardial perfusion imaging (MPI) is a functional imaging technique to confirm the diagnosis and assess the prognosis of coronary artery disease[1]. MPI is mostly performed with SPECT and PET imaging and aims to identify areas of the left ventricular myocardium with reduced perfusion by comparing a static perfusion scan in rest with a static perfusion scan in stress (i.e., exercise). During the MPI procedure, a radiolabeled tracer is administered intravenously. Common tracers are ^{99m}Tc-sestamibi or ^{99m}Tc-tetrofosmin in SPECT and ^{82}Rb or ^{13}N in PET MPI. A region in the perfusion scan with less than average number of detected photons can indicate a local perfusion deficit, as a result of a significant stenosis upstream. By performing both a scan in rest and stress, one can differentiate between a reversible or irreversible perfusion deficit, implying respectively ischemia or infarction[1–3].

Absolute, multimodal MPI has become a clinically relevant research topic within the cardiac imaging community[4,5]. Especially for PET the advantages of quantitative assessment in addition to qualitative, visual evaluation have been demonstrated[6]. Quantification of myocardial blood flow (MBF) and myocardial flow reserve provides a substantial advantage for diagnostic and prognostic evaluation of suspected or established coronary artery disease[4–7]. Currently these quantitative approaches are on the verge of being translated into the clinical workflow. In addition, similar approaches are also being explored for other imaging modalities, including CT, MRI, and SPECT. However, further efforts are necessary for on-site validation and to standardize measures across clinical centers, radiotracers, equipment, and software [7].

Medical Imaging 2022: Biomedical Applications in Molecular, Structural, and Functional Imaging,
edited by Barjor S. Gimi, Andrzej Krol, Proc. of SPIE Vol. 12036, 1203626
© 2022 SPIE · 1605-7422 · doi: 10.1117/12.2623667

1.2 Myocardial perfusion phantoms

Myocardial perfusion phantom studies can contribute to this unmet need for robust and on-site quality assessment due to the controlled setup and use of flow sensors providing a reference standard. Several left ventricular phantoms have been described in literature, in which various physiological states of perfusion can be simulated under static conditions, without flow[8,9]. In this, we observe an increasing trend in the use of 3D printing technology to obtain comprehensive representations of the heart[10–12]. Also, numerous perfusion phantoms have been proposed to facilitate physical flow standards for multimodal tissue perfusion imaging[13–15]. Nevertheless, current myocardial perfusion phantoms generally require in-house developed software for perfusion analysis. Evaluation of the entire absolute MPI application, i.e., both clinical hardware and software, involves an adequate phantom to mimic flow dynamics on the one hand and to make clinical software believe the phantom resembles a human heart on the other.

1.3 Research goal

Our main research goal encompasses the development of a myocardial perfusion phantom model to study MPI systems, and validate quantitative, multimodal MPI applications in a controlled setup (with reference flow measures). At this point, several steps have already been taken in our iterative phantom development process. We have started with designing, realizing, and testing of a proof-of-concept 3D printed left ventricular flow phantom that showed good compatibility with both clinical MPI hardware and software[16]. As a next step, we have incorporated in the following phantom iteration a novel concept for mimicking tracer kinetics[17], and performed initial tests with the phantom setup with SPECT-MPI. Then, we studied feasibility of the current setup for multimodal use (i.e., SPECT, PET, CT, and MRI), which showed promising results and provided us with new insights to improve multimodal phantom design (under review). The phantom evaluation as presented in this work builds on the previously developed phantom prototype and focuses on:

- Verifying the phantom design choices, including justification for a novel concept in mimicking tracer kinetics.
- Preliminary verification of initial phantom results in dynamic SPECT, involving comparison with a general two-tissue compartment model.

We want to take these insights into account in the development of the next, multimodal phantom prototype. Moreover, these steps in phantom evaluation support shaping of a suitable verification and validation strategy for the multimodal myocardial perfusion phantom design and realization.

2. PHANTOM DESIGN VERIFICATION

2.1 Requirements

Phantom design starts with drawing up the set of requirements. In this, we have aimed to minimize phantom complexity in order to maximize the reproducibility of phantom measurements. Henceforth, the main requirements for the myocardial perfusion phantom comprise:

1. Sufficient mimicking of the physical appearance of the heart, mainly the left ventricle, to enable phantom compatibility with dynamic, multimodal MPI hardware and software.
2. Adequate mimicking of the left ventricular flow to facilitate dynamic contrast measurement and derivation of arterial input functions (AIFs) that fall within a standardized normal and pathological patient range.
3. Advanced mimicking of myocardial perfusion to facilitate dynamic contrast measurement and derivation of tissue response functions (TRFs) that fall within a standardized normal and pathological patient range. This patient range entails a distinction between mimicking normal myocardial perfusion levels and gradations of regional perfusion deficits.

2.2 Design specifications

At this stage we have dedicated phantom development and evaluation to SPECT-MPI. Several phantom design specifications have evolved from the set of requirements (see Table 1), which are particularly focused on simulating a flow and perfusion component in such a way that it can be used for ground truth validation of clinical, quantitative MPI applications.

These design specifications can be divided in elements of physical appearance and functioning. In terms of physical appearance, the myocardial perfusion phantom is intended as a stationary cardiac insert for a commercial anthropomorphic thorax phantom. The insert ought to be made of materials that attain x-ray attenuation profiles in accordance with soft tissue, such as plastics. The cardiac insert is designed for 3D printing and consists of three cylindrical pieces (see Figure 1). The center part comprises a basic left ventricular cavity with an outlet that branches to three surrounding myocardial volumes. These identical volumes can be filled with tissue mimicking materials.

Phantom functioning is characterized by the incorporated flow dynamics in phantom and associated flow setup design. The overall setup (see Figure 2) comprises a closed loop flow circuit in which a fluid is circulated from the reservoir towards the phantom and back. The different components in the setup are connected with tubes. In this way, a (radiolabeled) contrast medium can be administered via a clinical contrast injector before entering the phantom. The phantom itself has a left ventricular cavity inlet and outlet, of which the outgoing flow is branched internally to the three myocardial volumes. These regions have individual outlets back to the reservoir. The flow can be regulated and measured in all parallel circuits using flow sensors and adjustable resistances. This setup primarily focuses on controlled mimicry of first-pass contrast kinetics by having a custom-built filter placed in the circuit that aims to prevent recirculation of contrast.

Table 1. Phantom specifications.

Properties	*Specifications*	*Symbol*	*Range and resolution*	*Unit*
Physical appearance	1. Stationary cardiac insert for commercial thorax phantom			
	2. Basic left ventricular shape of an average patient, comprising:			
	- a left ventricular cavity			
	- a flow inlet and outlet with branches to three identical, surrounding myocardial regions			
	3. Made of adequate materials for proper x-ray attenuation			
Functioning	4. Tunable fluid flow through the left ventricular cavity, specified by:	$\Phi_{ai}(t)$	4.0	L/min
	- a continuous flow of tap water with administered (radiolabeled) contrast kinetics			
	- the first pass of (radiolabeled) contrast kinetics			
	- accurate measurement of reference fluid flow			
	5. Tunable fluid flow through the myocardial regions, specified by:	$\Phi_{myo1\text{-}3}(t)$	[0.04 0.05 0.06 0.07 0.08]	L/min per myocardial region
	- a continuous, unidirectional fluid flow			
	- the first pass of (radiolabeled) contrast kinetics			
	- tunable myocardial uptake and retention			
	- accurate measurement of reference fluid flow			

We have applied a black box approach to obtain adequate, flow dependent time activity curve (TAC) outputs from phantom measurements with preset reference flows in the setup as inputs. Largely because of this black box approach, several simplifications have been made to functional phantom design in terms of simulating:

- flow dynamics,
- cardiac contraction dynamics, and
- tissue mimicking properties.

Regarding flow dynamics, we choose to generate a continuous instead of a physiological flow profile. In support of this simplification, patient TACs do not show fluctuations of a physiological flow profile either. An underlying cause is that TACs are based on average measured activities in a region of interest, which balances out fluctuations. In addition, measurement of the AIF concerns relatively fast kinetics of a respective small contrast volume (~2mL) in order to capture the contrast bolus within a single heartbeat. That is also why tap water is considered a sufficient blood mimicking fluid for current application with SPECT as the administration of a small radiotracer volume mixes well with the passing water. Another reason to simplify the phantom flow profiles is that the human coronary circulation has several mechanisms to facilitate a rather constant blood flow rate to the cells. This also reduces the presence of blood flow fluctuations in measured TRFs. In current phantom design, the coronary circulation is simplified into three 'coronary arteries' that open into three volumes and converge thereafter in three 'cardiac veins'. Unidirectional flow through these volumes represents both microcirculation and tissue perfusion. This generalization is based on how the relevant outputs are evaluated in clinical practice. Commonly, patient TRFs are assessed regionally and not locally. These curves consist of a combined (micro)vascular and tissue component. Ensuing MBF computation usually arises from compartment modeling. In this type of tracer kinetic modeling one of the main assumptions is that the concentration of tracer is equally distributed within the entire compartment[18]. In this, a correction factor is typically applied for the proportion of arterial tracer concentration in the measured TRF[19,20]. These arguments substantiate why a black box approach seems to suffice, provided that the measured tracer activity over time within the myocardial phantom region of interest corresponds to standardized patient tracer kinetics. Hence, a greater level of detail of the coronary circulation seems unnecessary to incorporate in phantom design.

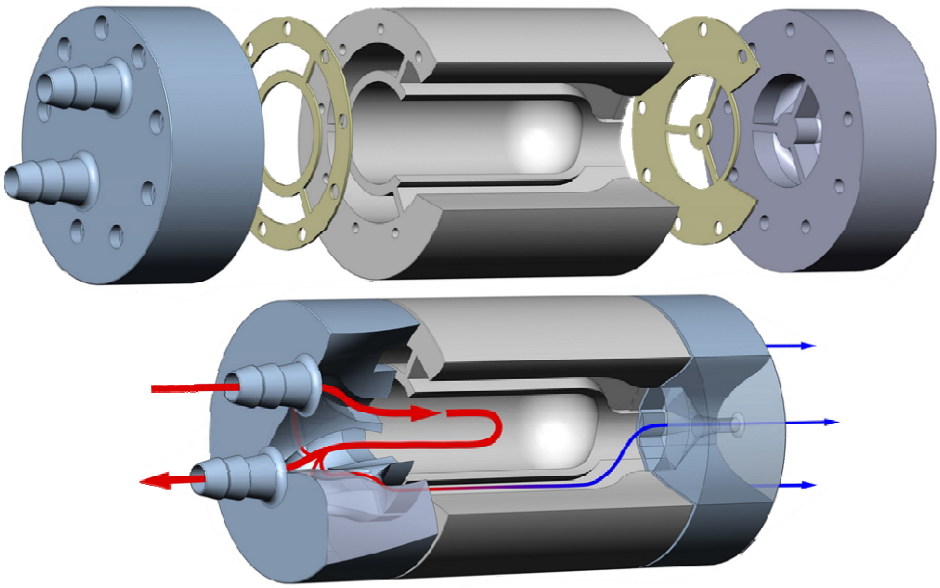

Figure 1. Myocardial perfusion phantom design. The exploded view (top) illustrates individual phantom parts. The three 3D printed pieces are fastened together with nylon screws with sealing in between for water proofing. The tailored cross section (bottom) visualizes inner phantom flow connections. The arrows indicate flow direction and magnitude, and its color differentiates between arterial input (red) and venous output (blue). The center phantom piece comprises the simulated left ventricular cavity and three surrounding myocardial volumes. These volumes are filled with tissue mimicking material during phantom fabrication. The two outer phantom pieces contain the inlet and outlet connection to the flow circuit and the internal branches to the myocardial volumes. The total phantom cylinder is designed to fit as cardiac insert in an anthropomorphic thorax phantom.

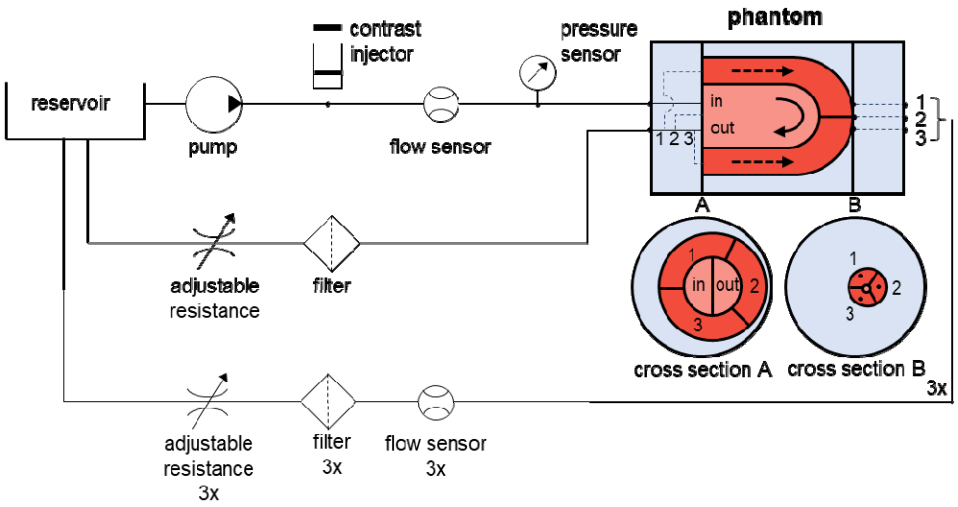

Figure 2. Phantom flow setup design.

A possible disadvantage of this black box approach can be that the simplified microcirculation and tissue mimicking properties are fine-tuned for a certain flow setting and may therefore show a different flow dependence than observed in patients. From that point of view it was decided to opt for standard flow settings within the phantom, hence also in mimicking normal perfusion and perfusion deficits. Normal reference flow is considered a cardiac output of 4.0 L/min and a flow through each myocardial phantom volume of 80 mL/min. This equates to a coronary flow of 6% of total cardiac output. A perfusion deficit is simulated by a reduced flow through one or multiple myocardial phantom regions by tuning the adjustable resistances. These settings comprise also a cardiac output of 4.0 L/min, and myocardial flows through each phantom myocardial volume of 40-80 mL/min (see Table 1). It is of importance to verify during phantom testing and evaluation whether the regulation and measurement of these flows are within the desired accuracy and reproducibility range (work in progress).

We have specified the degree of cardiac contraction dynamics desired to incorporate into phantom design. At this moment, it has been decided to build a stationary flow phantom. Although incorporation of cardiac contraction dynamics (and respiratory motion) will result in a more realistic phantom, it also entails great complexity in phantom realization. This will most likely go hand in hand with a decreased measurement reproducibility. It can be argued that the latter is also part of patient reality. However, at this stage, an outstanding measurement reproducibility is preferred over the degree of reality when it comes to developing a perfusion validation phantom.

In this phantom design we can alter the tissue mimicking properties by modifying the inlay of the myocardial volumes. Previous research by Kamphuis et al.[17] has demonstrated that sorbents can be used to fill the phantom tissue volumes in order to mimic tracer specific uptake and retention kinetics in the myocardium. This concept, as illustrated in Figure 3, can be approached with compartment modeling as well. Sorption is a physical and chemical process in which one substance, in our case the (radiolabeled) contrast medium, becomes (temporarily) attached to a selected sorbent or sorbent mixture[21]. In this, ion exchange and adsorption processes are of particular interest, as these can essentially mimic freely diffusible contrast kinetics in tissue, reversible binding of contrast media, and irreversible binding of contrast media to cells. As shown in Figure 3, the rate constants that describe contrast kinetics for a general two-tissue compartment model are comparable to the sorption and desorption rate constants that describe our physical phantom perfusion model. There is a small difference between the physiological and phantom model in how the tissue compartments are being represented, namely as a series or parallel connection between unbound and bound tissue compartments. This results in a distinctive derivation of tissue compartmental differential equations. Nonetheless, the slightly altered tissue-mimicking phantom design can be justified because in both cases image derived contrast kinetic measurement in tissues always comprises the sum of both tissue compartments. Hence, when solving the differential equations, the general analytical solutions of both sets of differential equations encompass a similar type of impulse response function (IRF)[22], as displayed in Figure 3. In this, $\alpha \neq \alpha'$ and $\beta \neq \beta'$.

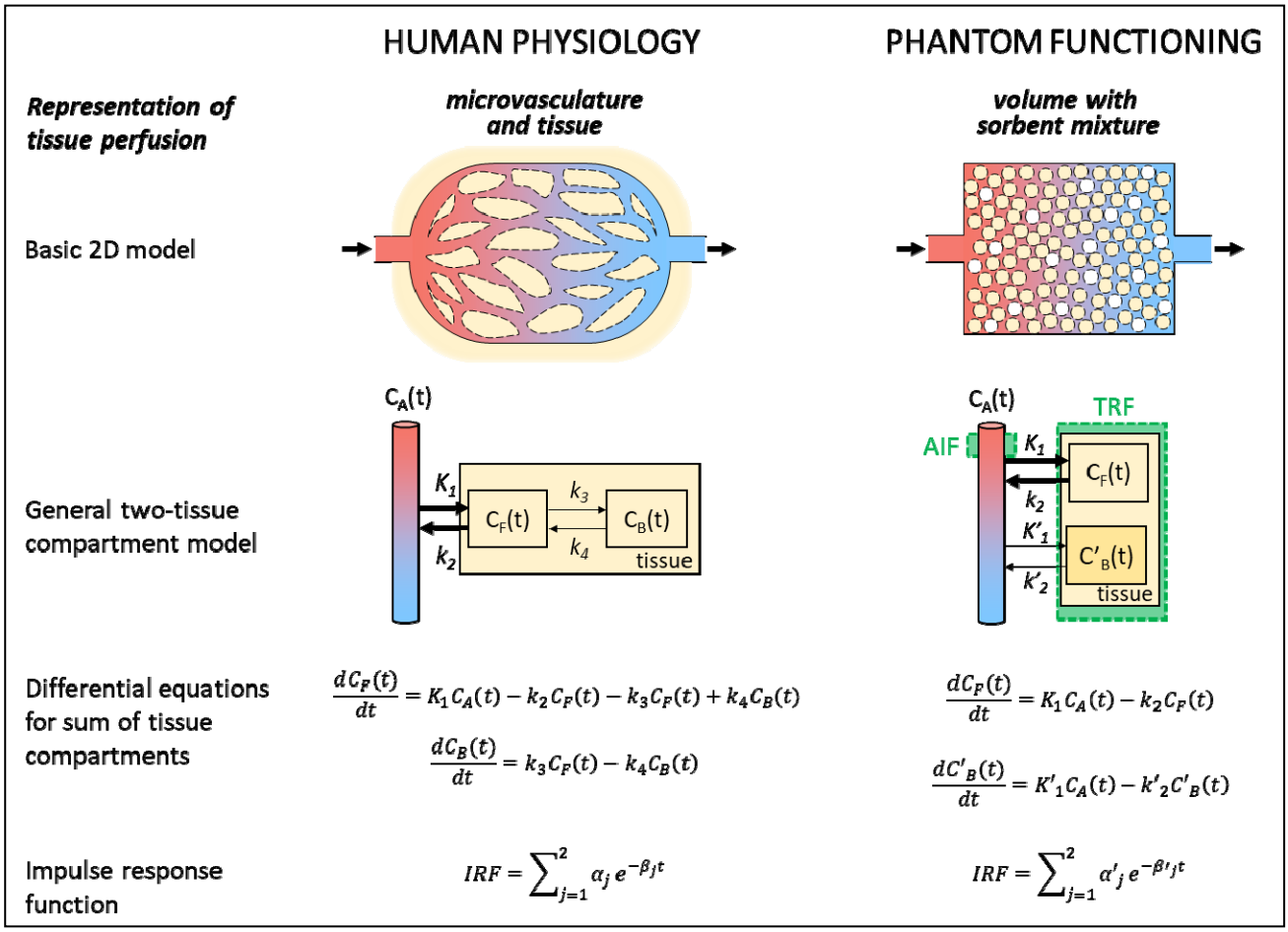

Figure 3. Schematic overview to illustrate a novel concept in mimicking contrast kinetics related to tissue perfusion in a physical phantom model. $C_A(t)$, $C_F(t)$, and $C_B(t)$ correspond to the contrast concentration measured / imaged over time in arterial blood, and free or bound in tissue, respectively. The illustrated phantom concept describes a similar relation between these measured concentrations using sorbents as tissue mimicking material. The rate constants that describe inter-compartmental contrast exchange rates are similar of nature for the physiological and phantom model, as can be seen by tissue derived differential equations and resulting impulse response function (see equation 1).

In the case of tracer kinetic phantom measurement with ^{99m}Tc labeled MPI tracers it is known that the first pass extraction fraction is around 55-65% of the total injected dose and is for a small fraction (1-5%) irreversibly trapped in myocardial tissue[23], hence k_3 = 0.01-0.05 min^{-1} and k_4 = 0 min^{-1}. Subsequently, the differential equations posed by this general two-tissue compartment model can be solved analytically using the Blomqvist approach[22]. This approach results in the following equation:

$$C_T = C_F + C_B = \frac{K_1}{k_2 + k_3}\left(k_2 e^{-(k_2+k_3)t} + k_3\right) \otimes C_A \tag{1}$$

In this, C_T comprises the tracer concentration in tissue over time, which is the sum of the tracer concentration freely diffused in tissue (C_F) and bound to cells (C_B). In general, the tissue concentration equals the convolution of the tracer concentration in the arterial blood component with its impulse response function (IRF). In our SPECT phantom measurements, we obtain an image derived and sampled tracer concentration time measurement from a region of interest in the LVC, i.e., the AIF (corresponding to $C_A(t)$), and in the myocardial phantom volumes. i.e., the TRFs (corresponding to $C_T(t)$). During phantom evaluation, we have assessed how changes in flow and tissue mimicking material compositions correlate with these theoretical model descriptions.

Figure 4. Overview of the phantom flow setup during initial phantom testing on a clinical SPECT system.

To be noted, phantom setup realization is described in a forthcoming publication.

3. INITIAL VERIFICATION OF PHANTOM RESULTS

3.1 Phantom measurements

Figure 4 shows an overview of the overall phantom setup during initial phantom testing in SPECT-MPI. In total, twenty-two phantom measurements were executed in dynamic SPECT-MPI spread over six, non-consecutive measurement days. In these measurements, the clinical protocol was followed completely, from dynamic image acquisition, tracer injection, image data reconstruction, to perfusion image visualization and quantitative perfusion analysis. Around 500 MBq of ^{99m}Tc tracer dissolved in 1.5 mL saline was injected at 1.0 mL/s just after initiating a standard 6 min dynamic scan. Figure 5 shows two examples of obtained phantom perfusion images, in which we varied myocardial flow and tissue mimicking properties. The methods used and results obtained with these phantom measurements are described in related work, which is currently under review. This work extends our current analysis by comparing the obtained AIF and TRFs with a patient example in combination with a general two-tissue compartment model.

3.2 Comparison with patient data

Figure 5 displays the mean AIF and TRF for similar phantom measurements compared to a patient example. The phantom measurements are very similar to the patient example. One of the observations was that a small percentage of tracer passed the filters in the flow setup and got recirculated into the phantom, as can be seen by the gradually upward trend in the average phantom TRF over time. The visible differences come from spillover effects in the patient data (in the AIF at $t \approx 30$s and in the TRF at $t \approx 15$s) and by a small fraction of recirculating tracer. This effect can be observed by a slightly increasing TRF over time, instead of the flattened line as observed in the patient example. The observed stronger increase in measured tracer activity in the patient TRF, including a higher peak activity, might also occur due to a higher flow.

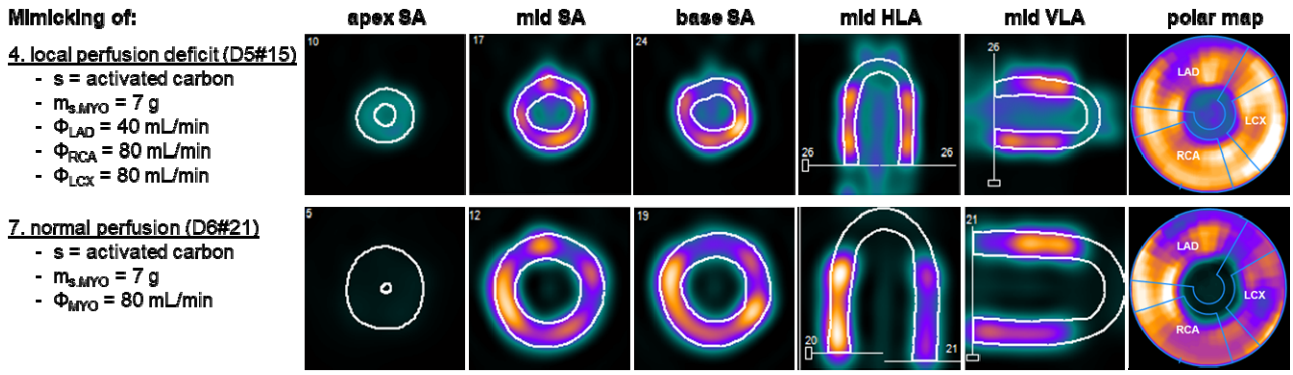

Figure 5. Two examples of myocardial perfusion imaging series aiming to highlight the overall phantom development and evaluation process. The image cross-sections and polar maps present the accumulated radiotracer distribution inside the phantom, which is a static representation of a dynamic time measurement. Note that the relative color scale is determined by default for each individual measurement and is therefore not linked between measurements. In these measurements, mimicking of radiotracer uptake, normal perfusion and perfusion deficit was examined using different parameter settings. Settings include the type and mass of sorbent (s) utilized to mimic myocardial tissue, and the amount of volume flux (Φ) directed through the myocardial segments (MYO). D5#15 stands for the measurement day and number, respectively. LAD = left anterior descending coronary artery, RCA = right coronary artery, LCX = left circumflex coronary artery, SA = short axis, HLA = horizontal long axis, and VLA is vertical long axis.

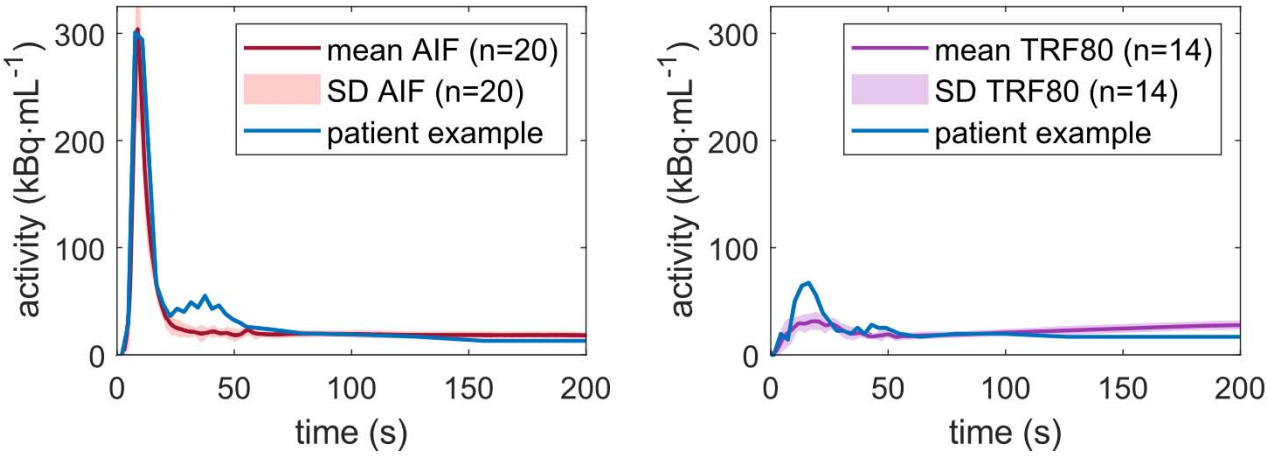

Figure 6. Time activity curve comparison between phantom data and a patient example. For the phantom data, the mean and standard deviation of the derived arterial input functions (AIFs) and tissue response functions (TRFs) at a flow of 80 mL/min were plotted.

3.3 Comparison with general two-tissue compartment model

We verified our phantom observations by fitting the analytical solution as proposed by Eq. 1 to our phantom data. As a starting point, we introduced a Gaussian AIF with characteristics similar to the AIFs observed in Fig. 6, i.e., a peak maximum of 300 kBq·min^{-1} at t = 15 s and a full-with at half maximum of 15 s. We have also incorporated a simplified scenario of tracer recirculation by introducing contrast recirculation in the simulated AIF building up to a continuous recirculation level of 10 kBq·min^{-1} from t = 15 s. For subsequent parameter estimation we used values from literature for k_3 and experimentally altered K_1 and k_2 to manually fit the data. Figure 7 visualizes the simulated AIF and TRF for different values for K_1 since this rate constant is most closely related to MBF. It should be noted that this model has been simplified in such a way that only K1 is varied, while in reality this is an interplay between all rate constants. However, for the purpose of initial phantom verification it was considered to be sufficient.

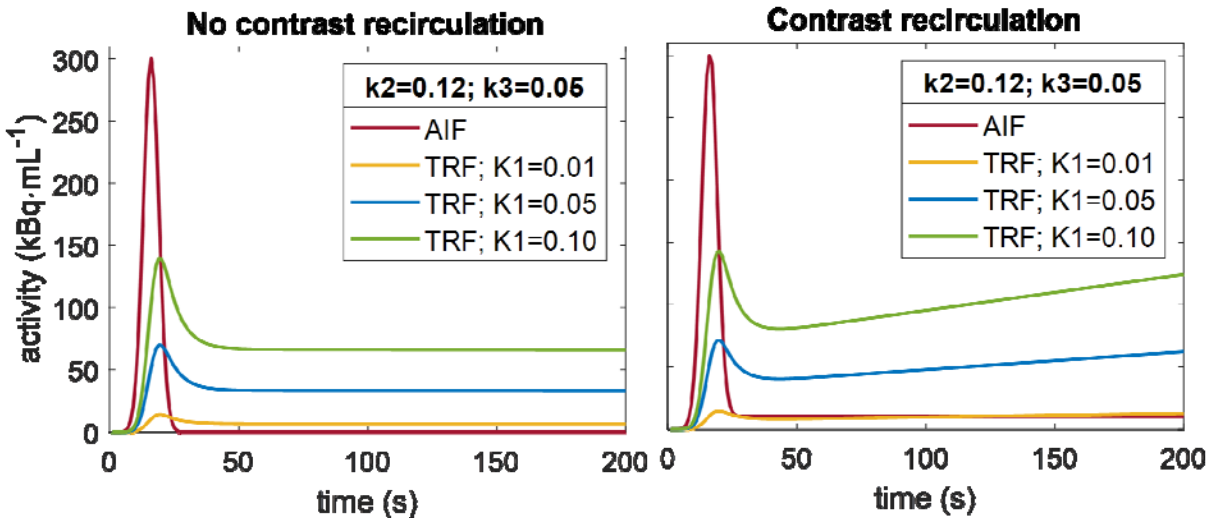

Figure 7. Time activity curve comparison between phantom data and a patient example. For the phantom data, the mean and standard deviation of the derived arterial input functions (AIFs) and tissue response functions (TRFs) at a flow of 80 mL/min were plotted.

When comparing the model data with phantom data we can indeed relate the upward trend in the phantom TRFs to the small extent of tracer recirculation. In addition, K1 (and presumably MBF) does affect the presence and height of the TRF peak around t=20s. In our current phantom setup, we observed a less dominant TRF peak, which may indicate a lower flow rate compared to the patient example and to our modeling results.

Verification of the obtained phantom data is still a work in progress. We also want to look at the different sorbent compositions that we used to empirically match the phantom TRFs with patient data and try to verify how these changes affect the rate constants.

4. CONCLUSION

With this work we have presented phantom evaluation. This concerned verification of the phantom design choices and initial verification of phantom results in SPECT by comparing the obtained tracer kinetic results with a patient example and corresponding tracer kinetic model. We have demonstrated that the rate constants that describe contrast kinetics for a general two-tissue compartment model are comparable to the sorption and desorption rate constants that describe the physical phantom. In line with this, sorbents have the capability to mimic detailed tracer specific kinetics, potentially up to the level of clinically derived MBF estimation. Moreover, we were able to verify some observations in phantom TRF data with preliminary simulation results. This part of phantom evaluation is still work in progress and underpins certain aspects of multimodal phantom redesign, but also supports shaping of a suitable verification and validation strategy for the multimodal myocardial perfusion phantom under development.

REFERENCES

[1] Hesse B., Tägil K., Cuocolo A., et al., "EANM/ESC procedural guidelines for myocardial perfusion imaging in nuclear cardiology," Eur J Nucl Med Mol Imaging 32(7), 855-897 (2005).

[2] Verberne H. J., Acampa W., Anagnostopoulos C., et al., "EANM Procedural Guidelines for Radionuclide Myocardial Perfusion Imaging with SPECT and SPECT / CT," (2015).

[3] Hyafil F., Gimelli A., Slart R.H.J.A., et al., "EANM procedural guidelines for myocardial perfusion scintigraphy using cardiac-centered gamma cameras," Eur J Hybrid Imaging 3(1) (2019).

[4] Dewey M., Siebes M., Kachelrieß M., et al., "Clinical quantitative cardiac imaging for the assessment of myocardial ischaemia," Nat Rev Cardiol. 17(7), 427-450 (2020).

[5] Sciagrà R., Lubberink M., Hyafil F., et al., "EANM procedural guidelines for PET/CT quantitative myocardial perfusion imaging," Eur J Nucl Med Mol Imaging, 48(4), 1040-1069 (2021).

[6] Cho S.G., Lee S.J., Na M.H., Choi Y.Y., Bom H.H.S., "Comparison of diagnostic accuracy of PET-derived myocardial blood flow parameters: A meta-analysis," J Nucl Cardiol., 27(6), 1955-1966 (2020).

[7] Murthy V.L., Bateman T.M., Beanlands R.S., et al., "Clinical quantification of myocardial blood flow using PET: Joint position paper of the SNMMI cardiovascular council and the ASNC. J Nucl Med.," 59(2), 273-293 (2018).

[8] Visser J.J.N., Sokole E.B., Verberne H.J., et al., "A realistic 3-D gated cardiac phantom for quality control of gated myocardial perfusion SPET: The Amsterdam gated (AGATE) cardiac phantom," Eur J Nucl Med Mol Imaging, 31(2), 222-228 (2004).

[9] Data Spectrum Corporation. Cardiac Insert. Product catablogues. http://www.orion-france.com/pdf/catalogues/Orion_Data_Spectrum.pdf. Published 2001. Accessed October 28, (2021).

[10] Grice J., Green S., Yuhas A., "An Improved 3D Printed Cardiac Phantom," J Nucl Med., 61 (2020).

[11] Abdullah K., McEntee M., Reed W., Kench P., "Development of an organ-specific insert phantom generated using a 3D printer for investigations of cardiac computed tomography protocols," J Med Radiat Sci., 65 (2018).

[12] Jin Z., Li Y., Yu K., et al., "3D Printing of Physical Organ Models: Recent Developments and Challenges," Adv Sci., 8(17), 2101394 (2021).

[13] Kok G., Pelevic N., Chiribiri A., et al., "A calibrated physical flow standard for medical perfusion imaging," Flow Meas Instrum., 78 (2021).

[14] Sun Nuclear Corporation. CT Perfusion Phantom. https://www.sunnuclear.com/products/ct-perfusion-phantom. Published 2021. Accessed October 28, 2021.

[15] Driscoll B., Keller H., Jaffray D., Coolens C., "Development of a dynamic quality assurance testing protocol for multisite clinical trial DCE-CT accreditation," Med Phys., 40(8), (2013).

[16] Kamphuis M.E., de Vries G.J., Verschoor J., et al., "Development of a dedicated 3D printed myocardial perfusion phantom: Proof-of-concept in dynamic SPECT," Med Biol Eng Comput. (2022).

[17] Kamphuis M.E., Kuipers H., Verschoor J., et al., "Development of a dynamic myocardial perfusion phantom model for tracer kinetic measurements, In print.

[18] Carson R.E., "Tracer kinetic modeling in PET. In: Positron Emission Tomography", Springer; 127-159 (2005).

[19] Leppo J.A., Meerdink D.J., "Comparison of the myocardial uptake of a technetium-labeled isonitrile analogue and thallium", Circ Res., 65(3), 632-639 (1989)

[20] Yoshida K., Mullani N., Gould K.L., "Coronary flow and flow reserve by PET simplified for clinical applications using rubidium-82 or nitrogen-13-ammonia," J Nucl Med., 37(10), 1701-1712 (1996).

[21] Seader J.D., Henley E.J., Roper D.K., etc., "Adsorption, Ion Exchange, Chromatography, and Electrophoresis," In: Separation Process Principles: Chemical and Biochemical Operations. 3rd ed. John Wiley & Sons (2010).

[22] Blomqvist G., Pauli S., Farde L., Eriksson L., Persson A., Halldin C., "Maps of receptor binding parameters in the human brain — a kinetic analysis of PET measurements," Eur J Nucl Med., 16(4), 257-265 (1990).

[23] Ballinger J.R., Koziorowski J., "Advances in Radiopharmaceuticals for Myocardial Perfusion Imaging". In: Ryder H, Testanera G, Veloso Jerónimo V, Vidovič B, eds. Myocardial Perfusion Imaging: A Technologist's Guide. EANM (2014).